



Bayesian denoising of wind tunnel tests using background noise measurements – application to supersonic jet noise

Nicolas Aujogue¹, Quentin Leclère¹, Jérôme Antoni¹, Emmanuel Julliard²

¹Univ Lyon, INSA Lyon, LVA, EA677, 69621 Villeurbanne, France
nicolas.aujogue@insa-lyon.fr

² Acoustics Department, Airbus Operations S.A.S., 31060 Toulouse, France

Abstract

A Bayesian method based on factor analysis is used to extract acoustic information from noisy cross-spectral matrices measured in a wind tunnel facility. Background noise measurements are incorporated as a prior probability distribution to infer the structure of the noise contaminating the signal. When using flush-mounted microphones on a wind tunnel, this technique allows the rejection of the hydrodynamic contribution due to the turbulent boundary layer developing on the walls of the test section as well as spurious sources of noise, while retaining only the acoustic part of the cross-spectral matrix due to the source of interest. The proposed method is applied on data measured on a model-scale dual stream aircraft engine operating at under-expanded conditions in a transonic wind tunnel. A wavenumber analysis of the considered test point shows that the denoised signals lend themselves well to acoustic imaging. It is shown that the signature of broadband shock-associated noise (BBSAN) is successfully separated from the background noise by inspecting the acoustic content of the denoised signals.

Keywords: denoising, broadband shock associated noise, Bayesian factor analysis.

1 Introduction

In the frame of aeroacoustic experiments aiming at localizing, quantifying and characterizing sources of noise, pressure signals are frequently acquired with microphone arrays placed directly inside the flow or flush-mounted on a rigid surface in order to sample the acoustic field as close as possible to its origin. In such situations, measurements are inevitably contaminated by noise: hydrodynamic perturbations and uninteresting acoustic waves may complicate the interpretation of the measurements and mask interesting components when applying acoustic imaging methods based on the measured cross-spectral matrix (CSM).

Hence, a number of denoising methods have been proposed to eliminate as much as possible of the noise while retaining only the acoustic signature of interest. Methods using the assumption of diagonal or sparse noise [1, 2, 3, 4] have proved successful in the high-frequency range where weak correlation is expected between pairs of microphones. When noise is highly correlated, further information may be used to achieve proper separation of signal and noise. For instance, the Coherent Output Power method [5, 6] uses additional sensors located outside of the flow to filter out hydrodynamic components. A different approach is adopted by Dinsenymer et al. [7], which combines factor analysis and a modelling of the TBL to infer the structure of the noise, thus avoiding the cost of additional hardware.

Whenever an independent background noise reference (measured by switching-off the source of interest) is available, it can be exploited to perform a relevant separation of signal and noise. The simplest approach consists in subtracting the background noise reference from the measured CSM (as in ref. [8], for instance), however, this method is known to be very sensitive to the quality of the background noise measurement especially when the signal-to-noise ratio (SNR) is very low, which is often the case in practical applications. It is in many cases very difficult to ensure that the reference CSM is perfectly equal to the noise CSM masking

the signal for two main reasons. First, estimation errors due to the finite length of the signals make the perfect equality of both CSMs impossible, since perfect convergence is never achieved. Second, small discrepancies between both setups (source switched-on and source switched-off) leads to a certain degree of variability of the CSM. These issues can cause the subtracted CSM to have negative autopowers or wrong phases on the cross-spectra. Efforts have been made to mitigate this issue by thresholding the subtracted CSM [9] or by identifying separate signal and noise subspaces before projecting the data onto the signal subspace [10], but their success generally rely on the accuracy of the reference background noise CSM.

Since the former scenario is often encountered in the context of flight tests or closed-section wind tunnel tests, the present works aim at exploiting the information contained in the structure of the background noise CSM, but regarding this structure as uncertain. The proposed approach thus allows the identified noise to slightly depart from the measured background noise reference. The Bayesian formalism is adopted, and a methodology similar to ref [11] is used, given the good results yielded by factor analysis on various benchmarks [12, 13]. In this context, the independent background noise reference is incorporated as a prior probability density in the model.

The second part of the article gives details about the inference method. In the third part of the article, this technique is used to denoise aeroacoustic signals measured in a transonic wind tunnel. Benefits for the characterization of the source are shown through acoustic imaging results.

2 Bayesian factor analysis

2.1 Data model

Final papers will be published in the conference proceedings. In the following, it is assumed that pressure signals are acquired with an array of M microphones. Measured signals are typically post-processed using Welch's method, which yields N_s snapshots of Fourier coefficients. Therefore, at each frequency bin, pressure may be represented as a collection of N_s vectors in \mathbb{C}^M : $(\mathbf{p}_i)_{(1 \leq i \leq N_s)}$. From a statistical point of view, pressure snapshots are considered as independent and identically distributed, since we consider stationary signals.

Let us decompose these vectors into a noise part $(\mathbf{n}_i)_{(1 \leq i \leq N_s)}$, and the acoustic signal of interest $(\mathbf{a}_i)_{(1 \leq i \leq N_s)}$:

$$\mathbf{p}_i = \mathbf{a}_i + \mathbf{n}_i, \quad 1 \leq i \leq N_s. \quad (1)$$

The idea behind factor analysis is that the statistical behavior of the M -dimensional signal may be well represented by a small number (say K) of random latent factors $(\mathbf{c}_i)_{(1 \leq i \leq N_s)}$. The weights linking the factors to the actual signal are gathered in a loading matrix \mathbf{L} , which is independent of the snapshot index:

$$\mathbf{a}_i = \mathbf{L}\mathbf{c}_i. \quad (2)$$

Thus, vector \mathbf{n}_i is the residual error between the factor analysis part and the measured data, and acts as a nuisance parameter.

Factor Analysis is an inference problem, since the statistical distribution of the factors and the residuals as well as the loading matrix, have to be determined from the available data. Here, a Bayesian point of view is adopted to solve this problem, which allows completing the available information –obtained from measurements–with prior knowledge of some parameters–obtained from additional measurements, user experience, theoretical considerations, or numerical computation, for instance. Complementary knowledge is introduced in the model using informative prior probability densities.

In the frame of aeroacoustic wind tunnel tests, it is common practice to perform dry runs to estimate background noise inside the facility. When microphones are flush-mounted on the wind tunnel wall, background noise may be composed of hydrodynamic perturbations caused by the turbulent boundary layer developing on the walls of the test section, and of parasite acoustic duct waves propagating inside the wind tunnel. The proposed denoising method uses background noise measurements to build the prior density of \mathbf{n} . With the preceding notation, one gets:

$$\mathbf{S}_{pp} = \mathbf{L}\mathbf{S}_{cc}\mathbf{L}^H + \mathbf{S}_{nn}, \quad (3)$$

where for snapshots of a given quantity \mathbf{x} , the empirical covariance matrix –also known as the Cross-Spectral Matrix (CSM)– is defined as $\mathbf{S}_{pp} = N_s^{-1} \sum_{i=1}^{N_s} \mathbf{x}_i \mathbf{x}_i^H$. In the above equation, cross-terms have been neglected. Background noise tests provide the experimenter with an estimate $\widetilde{\mathbf{S}}_{nn}$ of \mathbf{S}_{nn} .

2.2 Likelihood function

In the chosen data model, additive noise is assumed to behave as a centered complex Gaussian variable with covariance matrix \mathbf{S}_{nn} :

$$\mathbf{n}_i \sim \mathcal{N}_{\mathbb{C}}(\mathbf{0}, \mathbf{S}_{nn}). \quad (4)$$

Therefore, the likelihood function of the problem reads:

$$\mathbf{p}_i \sim \mathcal{N}_{\mathbb{C}}(\mathbf{L}\mathbf{c}_i, \mathbf{S}_{nn}). \quad (5)$$

2.3 Priors

In order to add sufficient parameterization to carry out a Bayesian inference, prior probability densities have to be assigned to all variables of the problem.

2.3.1 Factors

The factors are also given a centred complex Gaussian prior probability density with target covariance $[\gamma^2]$:

$$\mathbf{c}_i \sim \mathcal{N}_{\mathbb{C}}(\mathbf{0}, [\gamma^2]). \quad (6)$$

Since the target covariance matrix is diagonal, there is a priori no correlation between factors. Note that some correlation may be introduced in \mathbf{S}_{cc} by the effect of the likelihood function on the posterior probability of \mathbf{c}_i .

2.3.2 Variance of the factors

Since no prior information about the variance of the factors is available to the user, coordinates of γ^2 are also inferred. Their prior is set to an Inverse Gamma probability density function (p.d.f.) with parameters a , and b :

$$\gamma_k^2 \sim \mathcal{IG}(a, b), \quad 1 \leq k \leq K. \quad (7)$$

Parameters a and b are called hyper-parameters, and are set by the user. Since no information is available not the actual value of γ_k^2 , they should be set such that the prior has a very large variance. Since each

coordinate of γ^2 can have a different value, the model is heteroscedastic, which promotes sparsity among the factors.

2.3.3 Loading matrix

Each element of the loading matrix is assigned a centered complex Gaussian function with a constant variance $1/K$:

$$\mathbf{L}_{ij} \sim \mathcal{N}_{\mathbb{C}}\left(0, \frac{1}{K}\right). \quad (8)$$

2.3.4 Noise covariance matrix

Knowledge of the CSM of the noise can be exploited by setting a carefully chosen prior distribution for \mathbf{S}_{nn} , namely a complex Inverse-Wishart distribution with scale matrix $\widetilde{\mathbf{S}}_{nn} \times N_s$ and N_s degrees of freedom :

$$\mathbf{S}_{nn} \sim \mathcal{IW}_{\mathbb{C}}(\widetilde{\mathbf{S}}_{nn} \times N_s, N_s). \quad (9)$$

This particular choice of prior is motivated by the fact that the complex Inverse-Wishart distribution is the conjugate prior to the likelihood function. This means that the derivation of the posterior probability of \mathbf{S}_{nn} also yields a complex Inverse-Wishart distribution, from which samples can easily be drawn using Bartlett decomposition [14].

2.4 Overview of the inference method

The organization of the inference model can be summarized in a hierarchical graph shown in Fig. 1. Square boxes are deterministic variables, circular boxes are random variables to infer. Red boxes represent hyper-parameters, while blue boxes are not chosen by the experimenter. Parent-child relationships between variables are represented by the direction of the arrows: arrows point from parent to child nodes.

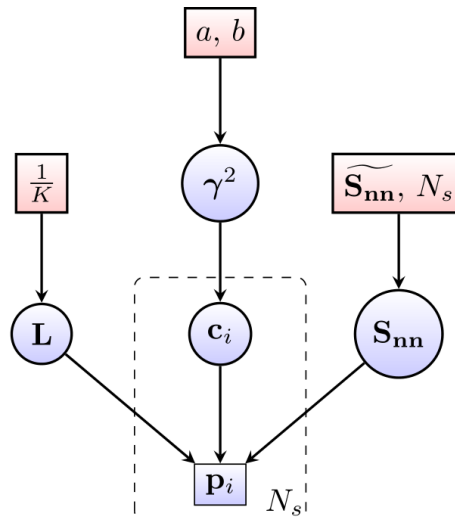


Figure 1 : Hierarchical graph of the model using plate notation.

The inference of unknown variables is achieved by drawing samples $\Theta^{(i)} = (\mathbf{S}_{cc}^{(i)}, \mathbf{L}^{(i)}, \gamma^{2(i)}, \mathbf{S}_{nn}^{(i)})$ from the posterior distribution of Θ . These samples are used to estimate the mean value of Θ after the algorithm has reached convergence. This inference method is a Monte-Carlo Markov chain algorithm (MCMC). A particular type of MCMC technique, namely a Gibbs sampling is implemented here. This method only requires the posterior conditional p.d.fs of the four elements of Θ . To derive the posterior conditional p.d.f. of a given variable Θ_j within a hierarchical model, the following relationship based on Bayes theorem is used [15]:

$$|\Theta_j|_{\infty_{-\Theta_j}} \propto [\Theta_j | \text{parents of } \Theta_j] \times \prod_k [\Theta_k | \text{parents of } \Theta_k] \quad (10)$$

The choice of the prior p.d.fs of the present model is made such that conjugate laws are used. In other words, the posterior conditional p.d.f. of all variables are of the same family as the prior law. The backbone of the Gibbs sampling of the unknown variables is shown in the pseudo-code below. Typically, a thousand iterations are necessary at each frequency. Depending on the number of microphones and factors, this algorithm runs in a few dozen seconds up to a few minutes on a modern laptop computer. In any case, this is negligible compared to the typical time and budget dedicated to an aeroacoustic test campaign.

```

Input:  $\mathbf{S}_{pp}, \widetilde{\mathbf{S}}_{nn}, K, N_s, a, b, i_{max}$ 
Initialization:  $\Theta^{(0)}$ 
while  $i < i_{max}$  do
  for  $j < 4$  do
     $\Theta_j^{(i+1)} \leftarrow [\Theta_j^{(i)} |_{\infty_{-\Theta_j^{(i)}}}]$ 
  end
  save  $\Theta^{(i+1)}$ 
   $i \leftarrow i + 1$ 
end

```

Algorithm 1: Gibbs sampling of the variables of the proposed model

3 Experimental setup



Figure 2 : Overview of the test section. The red zone is a zoom of the nozzle. The green zone shows the rail where the microphones are flush-mounted.

The considered data was measured during a test campaign aiming at characterizing broadband shock-associated noise generated by dual-stream aircraft engines in the presence of flight effects. Test were carried out on a scaled aircraft engine nozzle placed in a transonic wind tunnel of section 66×66 inches. The

nozzle is designed to reproduce the flow characteristics of a Rolls-Royce Trent 500 engine. The ambient flow in the wind tunnel is set to Mach 0.85, which is representative of a cruise flight Mach of a long-haul aircraft. In order to reproduce the signature of a real engine, the dual-stream architecture of the jet was mimicked by using three separate flows. The primary flow is composed of a mixture of helium and air to simulate the effect of heating by the core of the engine [16], while the ventilation, secondary, and ambient flows are only composed of air.

The instrumentation is composed of a linear array of 129 irregularly spaced microphones visible in the green zone in Fig. 2. Since microphones are flush-mounted on a metallic rail placed directly inside the flow, the measured acoustic field is expected to be corrupted by strong additive noise due to the turbulent boundary layer developing on the surface of the rail. In addition, although special care was given to minimize the generation of parasite acoustic waves inside the test section [17], residual acoustic noise is still present. The purpose of this study is to remove as much as possible both contributions from the measurements in order to isolate BBSAN. Signals were synchronously acquired at a sampling rate of 102.4 kHz, and CSMs were computed with 100 Hz resolution using Welch's method ($N_s \approx 650$). The Strouhal number S_t , the equivalent jet diameter D_j and equivalent jet velocity U_j are used to normalize the data, and are computed according to standard ARP876F.

4 Results

In Fig. 3, all autospectra are plotted as a function of frequency. Humps corresponding to the signature of the engine are visible in the raw autospectra, but are mostly masked by the TBL, which seriously limits the

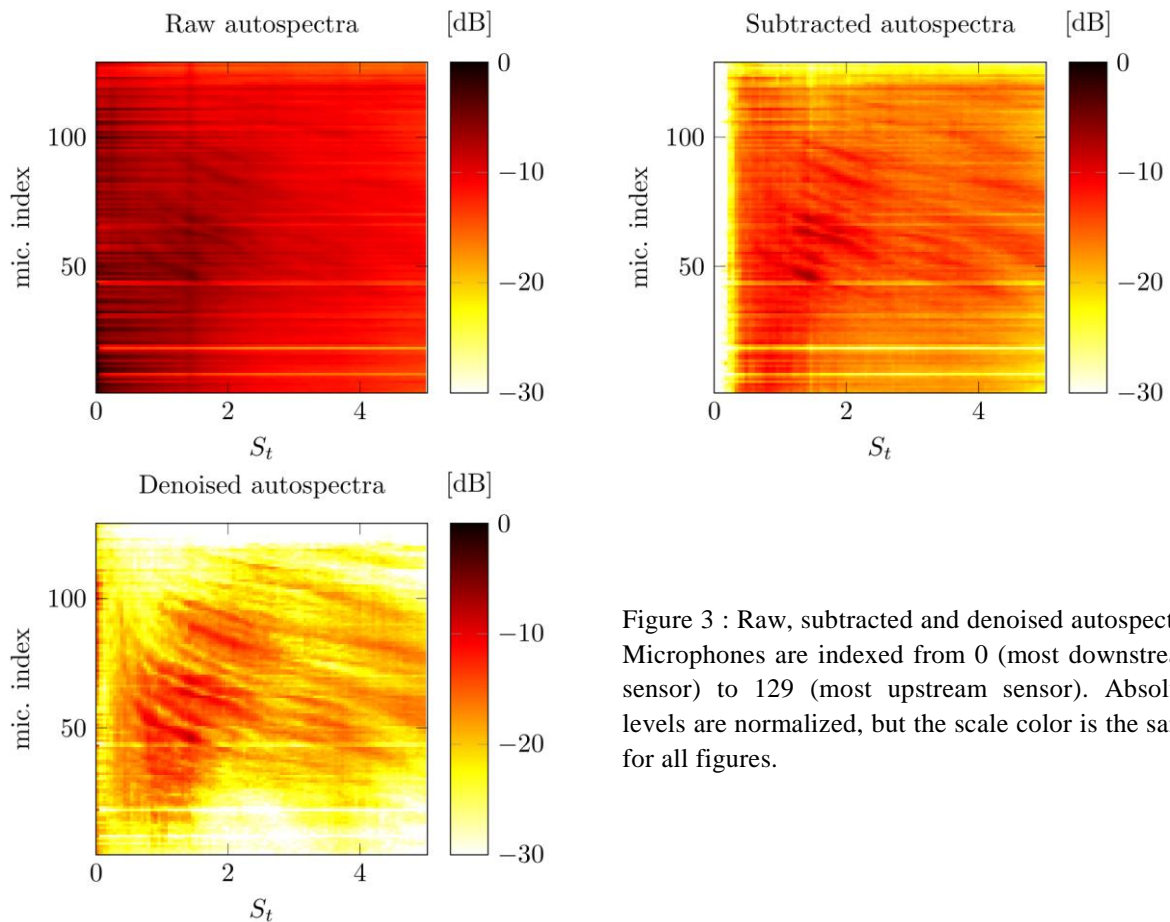


Figure 3 : Raw, subtracted and denoised autospectra. Microphones are indexed from 0 (most downstream sensor) to 129 (most upstream sensor). Absolute levels are normalized, but the scale color is the same for all figures.

dynamic range. Moreover, for some microphones, discrepancies in the overall level can be noticed. They are due to small manufacturing imperfections on the flushness of the microphones. Subtracted autospectra show better dynamics, which makes the contribution of the engine easier to see. However, in the low-frequency range, some autospectra are negative, and the corresponding CSMs are negative-definite, which is not physically possible. Further analysis of the setup show that the repeatability error is of the order of 0.8 dB. Therefore, the subtraction method has a limited practical ability to extract the relevant part of the CSM, especially when the SNR is very low, i.e. when the signal part is of the same order magnitude as the repeatability error. Signals denoised with the proposed method show improved behavior. The directivity pattern of the jet is clearly identified. The frequency-dependent directivity observed on the autospectra is an expected behavior of BBSAN, indicating that the extracted signal is relevant.

Fig. 4 shows the frequency-wavenumber analysis of raw, subtracted and denoised signals. The maps are computed using Bayesian focusing [18] with a Tikhonov regularization. A source prior density is taken into account, and computed using beamforming coherence defined as:

$$v_k^2(\mathbf{S}_{pp}) = \frac{\mathbf{w}_k^H \mathbf{S}_{pp} \mathbf{w}_k}{\mathbf{w}_k^H \mathbf{C}_p \mathbf{w}_k} \quad (11)$$

Where \mathbf{w}_k is a vector containing the signature of a plane wave with normalized axial wavenumber $\tilde{k} = k \times D_j$. The advantage of wavenumber analysis is that it provides a natural way of separating the TBL components from the acoustic signal, since they are located in different zones of the $\tilde{k} - S_t$ map. The limits of the acoustic domain are shown with solid lines in Fig. 4a, 4b, and 4c. Components outside of this domain cannot be due to propagative acoustic waves, and are mainly due to the TBL, concentrated around the convective ridge shown by the dotted line. Components inside the acoustic domain can either be due to the contribution of the engine, or to other parasite acoustic waves propagating inside the test section. With this in mind, one can get a rough estimate of the acoustic CSM by applying a filter in the wavenumber domain,

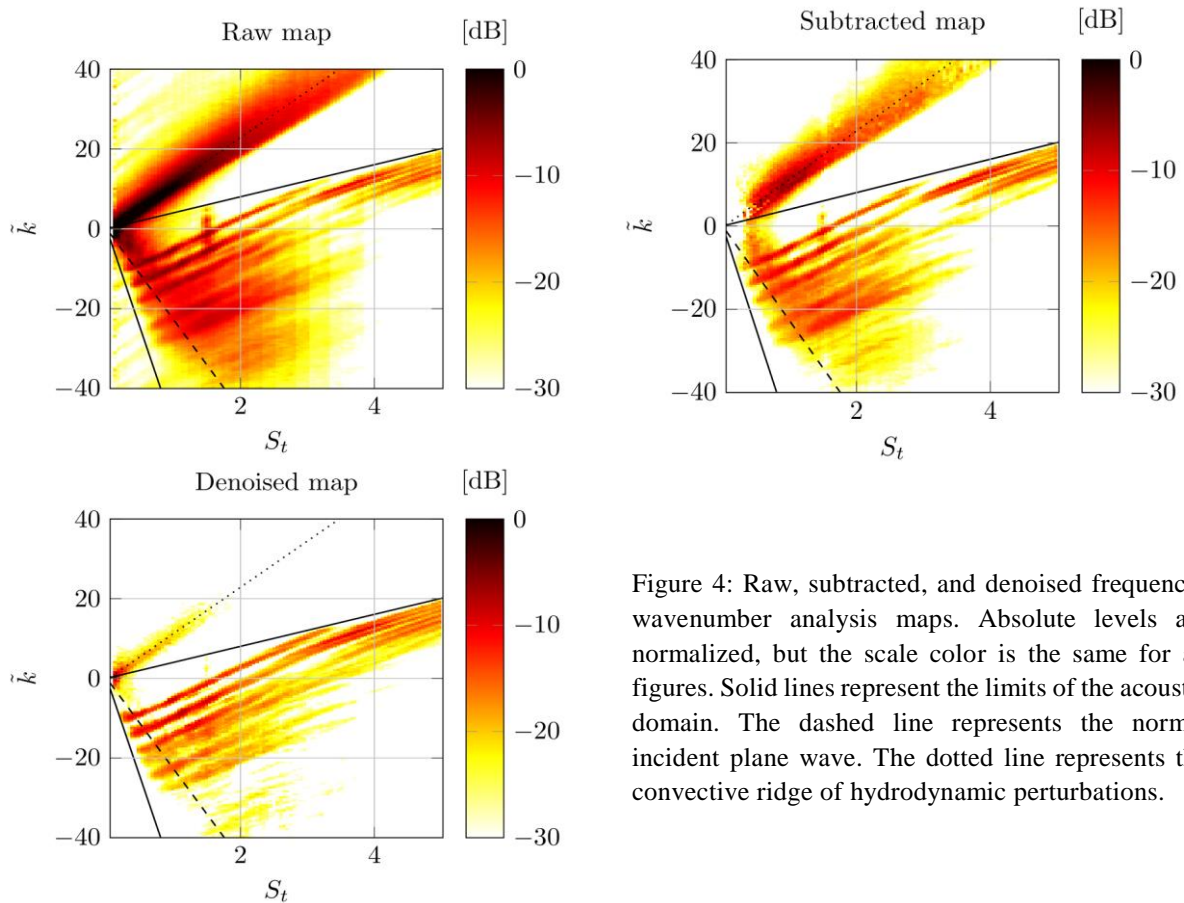


Figure 4: Raw, subtracted, and denoised frequency-wavenumber analysis maps. Absolute levels are normalized, but the scale color is the same for all figures. Solid lines represent the limits of the acoustic domain. The dashed line represents the normal incident plane wave. The dotted line represents the convective ridge of hydrodynamic perturbations.

and using it as a reference to assess the quality of the denoising. Note that this filtering method is only made possible by the favorable configuration of the setup, and may be impossible in more complex configurations because of aliasing due to insufficient sampling in the axial direction or when it is impossible to install a line of microphones parallel to the jet, such as in flight tests.

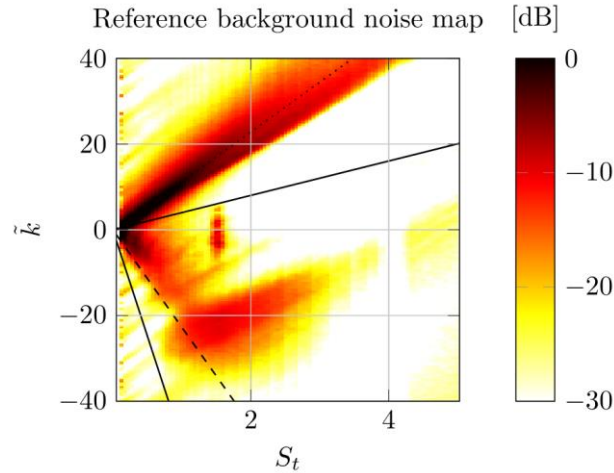


Figure 5: Reference background noise frequency-wavenumber analysis maps.

Fig. 4a shows that most of the energy contained in the CSM is due to the turbulent boundary layer, since the major part of the energy is localized near the convective ridge. As mentioned above, $\tilde{k} - S_t$ maps make it possible to separate hydrodynamic contributions from the signature of the engine located in the acoustic domain. The latter is composed of a sum of discrete ridges. According to Tam and Tanna's distributed source model [19], their slopes give indications about the convection velocity of the turbulent eddies inside the jet, and their intercepts are linked to the spatial organization of the shock-cell pattern located downstream the nozzle. Fig. 4b shows that subtracting the reference background noise CSM fails at suppressing the hydrodynamic content of the CSM, since a large part of the power is still located outside of the acoustic region. In order to be able to process the signals in the low-frequency region, the subtracted CSM was artificially made positive-definite by projecting the raw CSM onto eigenvectors of the background noise reference CSM and by thresholding the subtracted eigenvalues to zero. It seems that too much acoustic energy is left in the subtracted map, because the acoustic signature of the background noise shown in Fig. 5 is still visible on the subtracted map, and overlaps the BBSAN contribution. The acoustic content of the background noise reference is composed of a large hump located mainly at negative wavenumbers, and of a peak centered at $(\tilde{k}, S_t) = (0, 1.5)$. These acoustic waves are likely due to mixing jet noise originating from the inner and outer mixing layers of the co-axial (subsonic) flows, as well as from the wake of the pylon. In Fig. 4c, most of the TBL part is efficiently removed, except for very low Strouhal numbers. The proposed denoising method has the advantage of yielding positive-definite CSMs, which avoids applying additional post-processing to artificially remove the non-physical components of the CSM. In order to quantify the quality of the denoising, the ratio between the amount of energy inside the acoustic domain can be compared to the amount of hydrodynamic energy by integrating the sources on corresponding \tilde{k} zones. This indicator is designed to check that the residual CSM only contains acoustic energy. Fig. 6a shows that for raw signals, the TBL contribution is 5 dB higher than the acoustic contribution up to $S_t = 4$. For $S_t > 4$, the TBL ridge is outside of the scanned \tilde{k} region, therefore, the TBL level artificially drops, thus reducing the value of the considered indicator. The subtraction method only allows to decrease the TBL/acoustic ratio to 0 dB, indicating that half of the energy of the CSM is still due to hydrodynamic noise. On the contrary, the proposed denoising method allows to reduce the TBL contribution at least 10 dB below the acoustic

contribution for $S_t > 0.2$. The TBL vs acoustic ratio is further decreased to -20 dB for higher frequencies, indicating that the CSM is essentially composed of acoustic contributions.

The levels of acoustic energy can also be checked to understand how much of the acoustic energy is removed from the original CSM. Fig. 6b shows that the subtraction of the reference CSM reduces the overall acoustic energy of around 5 dB below $S_t = 3$. This is due to the fact that this method partially suppresses the broadband hump of the reference CSM centered at $(\tilde{k}, S_t) = (-25, 1.5)$ as well as the peak centered at $(\tilde{k}, S_t) = (0, 1.5)$, although a small part of them are still present in the CSM (see Fig. 4b). The denoised signals exhibit slightly smaller acoustic levels because the residual background noise is more efficiently removed than in the subtracted signals, since the present method allows the identified noise to be slightly different from the reference CSM. It can be noticed however that the peak at $S_t = 1.5$ is still visible, showing that this source of noise is not perfectly removed.

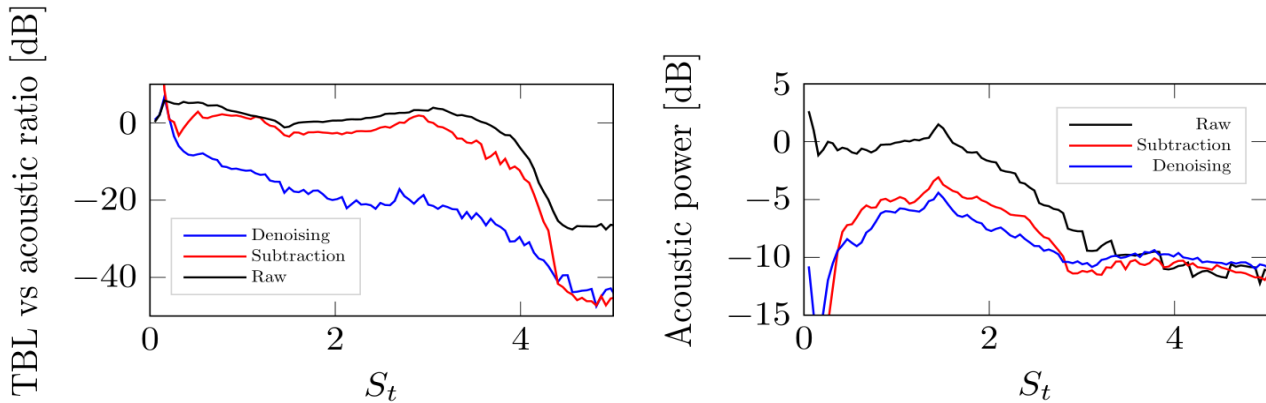


Figure 6: Top figure shows the ratio of TBL versus acoustic content in the residual CSM. Bottom figure shows the normalized acoustic level identified by the methods.

The conclusion that can be drawn from Figs. 6a and 6b is that the subtracted CSM is dominated to a large extent by hydrodynamic fluctuations that mask the acoustic contribution of interest. To the contrary, TBL is almost completely removed by the proposed method, and the denoised acoustic part is similar to the one identified in the subtracted CSM, apart from a few dBs of difference explained by the small variability of the background noise between the two measured configurations.

5 Conclusion

A denoising method was introduced to efficiently separate the acoustic contribution from uninteresting background noise components (TBL or parasite acoustic sources) in the context of aeroacoustic testing. It is based on Bayesian factor analysis with a structured noise, whose characteristics have been estimated by measuring an independent reference CSM. Unlike methods from the literature, the measured background noise reference is seen as uncertain, and the identified noise is allowed to slightly depart from it, thus providing additional flexibility to identify a relevant signal. Experimental results on a scaled dual-stream engine in a transonic wind tunnel show that the proposed method allows efficient removal of the TBL contribution. It also highlights that this technique outperforms the crude but common subtraction method, which consists in subtracting the background noise reference CSM from the measurement. Future works might focus on exploiting the full potential of Bayesian denoising by tackling more complex configurations where wavenumber filtering does not suffice to extract a rough estimate of the acoustic contribution of interest.

Acknowledgements

This work was supported by the LABEX CeLyA (ANR-10-LABX-0060) of Université de Lyon, within the program "Investissements d'Avenir" (ANR-16-IDEX-0005) operated by the French National Research Agency (ANR).

References

- [1] J. Hald, "Removal of incoherent noise from an averaged cross-spectral matrix," *The Journal of the Acoustical Society of America*, vol. 142, no. 2, pp. 846–854, 2017.
- [2] R. Dougherty, "Cross spectral matrix diagonal optimization," in 6th Berlin Beamforming Conference, Feb. 2016.
- [3] Q. Leclère, N. Totaro, C. Pezerat, F. Chevillotte, and P. Souchotte, "Extraction of the acoustic part of a turbulent boundary layers from wall pressure and vibration measurements," in *Proceedings of the International Congress on Noise and Vibration Emerging Methods, Proceedings of Novem 2015*, (Dubrovnik, Croatia), p. 49046, 2015.
- [4] S. Amailland, J.-H. Thomas, C. Pézerat, and R. Boucheron, "Boundary layer noise subtraction in hydrodynamic tunnel using robust principal component analysis," *The Journal of the Acoustical Society of America*, vol. 143, no. 4, pp. 2152–2163, 2018.
- [5] I. Davis and G. Bennett, "Experimental investigations of coherence based noise source identification techniques for turbomachinery applications-classic and novel techniques," in 17th AIAA/CEAS Aeroacoustics Conference (32nd AIAA Aeroacoustics Conference), p. 2830, 2011.
- [6] Q. Leclere, A. Dinselmeyer, J. Antoni, E. Julliard, and A. Pintado-Peno, "Thresholded multiple coherence as a tool for source separation and denoising: Theory and aeroacoustic applications," *Applied Acoustics*, vol. 178, p. 108021, 2021.
- [7] A. Dinselmeyer, Q. Leclère, J. Antoni, and E. Julliard, "A bayesian approach for the separation of the acoustic and the correlated aerodynamic wall pressure fluctuations," *The Journal of the Acoustical Society of America*, vol. 149, no. 6, pp. 4410–4421, 2021.
- [8] J. Huber, K. Britchford, E. Laurendeau, V. Fleury, J. Bulté, A. Sylla, and D. Long, "Understanding and reduction of cruise jet noise at model and full scale," in 15th AIAA/CEAS Aeroacoustics Conference (30th AIAA Aeroacoustics Conference), p. 3382, 2009.
- [9] C. J. Bahr and W. C. Horne, "Subspace-based background subtraction applied to aeroacoustic wind tunnel testing," *International Journal of Aeroacoustics*, vol. 16, no. 4-5, pp. 299–325, 2017.
- [10] J. Bulté, "Acoustic array measurements in aerodynamic wind tunnels: a subspace approach for noise suppression," in 13th AIAA/CEAS Aeroacoustics Conference (28th AIAA Aeroacoustics Conference), p. 3446, 2007.
- [11] A. Dinselmeyer, J. Antoni, Q. Leclère, and A. Pereira, "A probabilistic approach for cross-spectral matrix denoising: Benchmarking with some recent methods," *The Journal of the Acoustical Society of America*, vol. 147, no. 5, pp. 3108–3123, 2020.
- [12] P. Sijtsma, A. Dinselmeyer, J. Antoni, and Q. Leclere, "Beamforming and other methods for denoising microphone array data," in 25th AIAA/CEAS Aeroacoustics Conference, p. 2653, 2019.
- [13] A. Dinselmeyer, J. Antoni, Q. Leclère, and A. Pereira, "On the denoising of cross-spectral matrices for (aero) acoustic applications," in *bebec*, 2018.
- [14] D. K. Nagar and A. K. Gupta, "Expectations of functions of complex wishart matrix," *Acta applicandae mathematicae*, vol. 113, no. 3, pp. 265–288, 2011.
- [15] W. M. Bolstad, *Understanding computational Bayesian statistics*, vol. 644. New York: John Wiley & Sons, 2009.
- [16] D. Long, "Turbofan exhaust noise using helium/air mixture to simulate core temperature," in 10th AIAA/CEAS Aeroacoustics Conference, p. 3018, 2004.

- [17] D. Long, “Acoustic testing in transonic wind tunnels,” in 44th AIAA aerospace sciences meeting and exhibit, p. 921, 2013.
- [18] J. Antoni, “A bayesian approach to sound source reconstruction: Optimal basis, regularization, and focusing,” *The Journal of the Acoustical Society of America*, vol. 131, no. 4, pp. 2873–2890, 2012.
- [19] C. K. Tam and H. Tanna, “Shock associated noise of supersonic jets from convergent-divergent nozzles,” *Journal of Sound and Vibration*, vol. 81, no. 3, pp. 337–358, 1982.